A thermodynamic, electrochemical and molecular dynamics study on NAD and NADP recognition by 1,4,7,10,13,16,19-heptaazacyclohenicosane ([21]aneN$_7$)†

Antonio Doménech,[a] Enrique García-España,*[a] José A. Ramírez,[a] Bernardo Celda,*[b] Mª Carmen Martínez,[b] Daniel Monleón,[b] Roberto Tejero,[b] Andrea Bencini[c] and Antonio Bianchi*[c]

[a] *Department of Inorganic Chemistry, University of Valencia, C/ Dr. Moliner 50, 46100 Burjassot (Valencia), Spain*
[b] *Department of Physical Chemistry, University of Valencia, C/ Dr. Moliner 50, 46100 Burjassot (Valencia), Spain*
[c] *Department of Chemistry, University of Florence, Via Maragliano 75/77, 50144 Florence, Italy*

Received (in Cambridge) 30th July 1998, Accepted 30th October 1998

Interaction of the macrocyclic polyamine 1,4,7,10,13,16,19-heptaazacyclohenicosane ([21]aneN$_7$) in its protonated forms with the dinucleotides NAD^+ and $NADP^+$ has been followed by pH-metric titration, NMR and cyclic voltammetry. Both dinucleotides interact strongly with [21]aneN$_7$ forming adduct species with protonation degrees varying from 3 to 7 for NAD^+ and from 3 to 8 for $NADP^+$. Plots of the overall amount of complexed species show recognition of $NADP^+$ over NAD^+ throughout a wide pH range. The extra phosphate group attached to the ribose moiety of $NADP^+$ seems to be the factor controlling the recognition process as proved by ^{31}P NMR studies. Molecular dynamics on the adducts formed between NAD^+ and $NADP^+$ and tetraprotonated [21]aneN$_7$ confirm the participation of the phosphate appended to the ribose moiety of the adenosine nucleoside in the electrostatic and hydrogen bonding interactions. Cyclic voltammetric measurements denote significant alterations in the electrochemical behaviour of the NAD^+/NADH or $NADP^+$/NADPH couples as a function of the interaction between the dinucleotide and receptor.

Introduction

Interaction of polyammonium receptors with polycharged anionic species through non-covalent forces often results in the formation of supramolecular adducts displaying well-characterised chemical properties. In this respect, over the last two decades, much attention has been devoted to the interactions of macrocyclic polyammonium receptors with phosphate type anions and particularly with nucleotides like ATP, ADP or AMP.[1] In many instances it was found that the formation of the non-covalent host–guest complex brought about important rate accelerations of the ATP hydrolysis into ADP and inorganic phosphate. In this respect macrocycles 1,4,7,13,16,19-hexaaza-10,22-dioxatetracosane (bisdien) and 1,4,7,10,13,16,19-heptaazacyclohenicosane ([21]aneN$_7$) have proved to be the most efficient catalysts.[2,3]

However, studies on the interaction of the ubiquitous nucleotides NAD^+ and $NADP^+$ with polyammonium receptors are very scarce.[4] One of the most significant works in this sense is a recent paper of Lehn *et al.*[5] in which it is reported that macrocycles derived from bisdien by mono- or bifunctionalisation with acridine moieties were able to recognise nucleotide and dinucleotide anions through a variety of intermolecular forces. NAD^+ and $NADP^+$ play a crucial role in a large variety of redox processes involved in most metabolic routes. In spite of the similarities between both coenzymes, $NADP^+$ differs structurally from NAD^+ only by the presence of an additional phosphate group esterified to the 2′-hydroxy group of its AMP moiety (see Scheme 1), they are used differently in the metabolic redox processes. While NAD^+ participates almost exclusively in oxidative degradations that yield ATP, $NADP^+$ is confined with few exceptions to the reductive biosynthesis. It is the presence of the extra phosphate group in $NADP^+$ that permits the proteins to differentiate between both coenzymes, which constitutes a clear example of molecular recognition in biochemical reactions. NAD and NADP cofactors are linked to the proteins through a variety of weak intermolecular forces. Among them, electrostatic interactions or/and hydrogen bonding with lateral chains of basic amino acids like arginine or lysine seem to be well defined features in these domains.[6] It is certain that these interactions are modulating the redox properties of these dinucleotides contributing to the specificity of a determined enzyme.

Here we report on the interaction of the polyammonium receptor 1,4,7,10,13,16,19-heptaazacyclohenicosane ([21]aneN$_7$)[7] with $NADP^+$ and NAD^+ nucleotides (see Scheme 1) and we show that this receptor, in its protonated forms, is able to recognise $NADP^+$ over NAD^+ throughout a wide pH range. In order to gain more insight about the factors contributing to the selective recognition of $NADP^+$ over NAD^+ by [21]aneN$_7$, a wide set of energy minimisation, torsion angle search and molecular dynamics calculations have been carried out on the interaction of the dinucleotides with $H_4([21]aneN_7)^{4+}$.

Experimental

Materials

[21]aneN$_7$ was synthesised as described in ref. 7 and handled as

† Supplementary data (SUPPL. 57457, pp. 1) are available from the British Library. For details of the Supplementary Publications Scheme, see 'Instructions for Authors', *J. Chem. Soc.*, *Perkin Trans. 2*, available *via* the RSC Web page (http://www.rsc.org/authors). The supplementary data is also available on the RSC's web server (http://www.rsc.org/suppdata/perkin2/1999/23/).

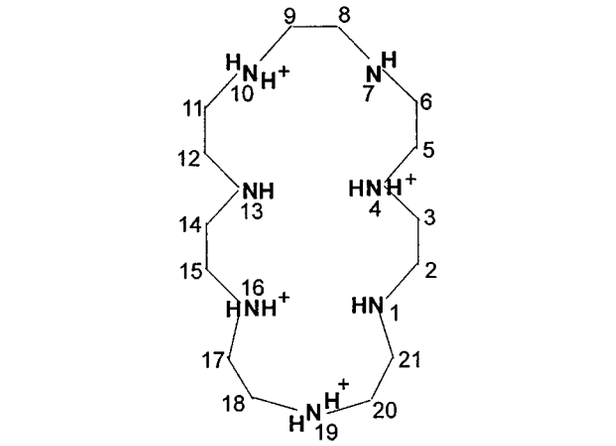

$H_4([21]aneN_7)^{4+}$

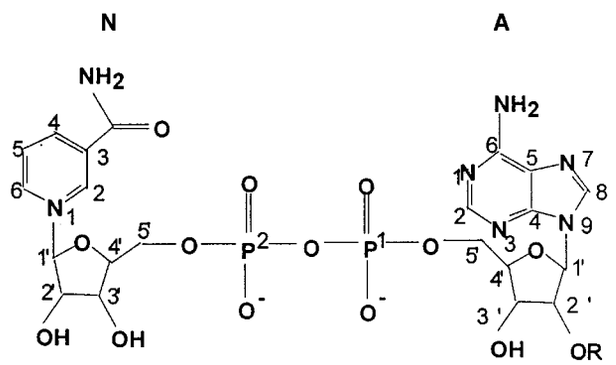

NAD$^+$ R = H
NADP$^+$ R = $P^3O_3^{2-}$

Scheme 1 Receptor and substrate molecules.

its heptahydrochloride salt. β-Nicotinamide adenide dinucleotide sodium salt (HPLC > 98%), β-nicotinamide adenine dinucleotide phosphate monohydrate and β-nicotinamide adenide dinucleotide reduced disodium salt (HPLC > 97%) were Fluka reagents. The concentration of the dinucleotides was accurately determined by potentiometric titration. $NaClO_4$ used as supporting electrolyte was purified according to a published procedure.[8] All the other chemicals were Merck reagent grade, and were used without further purification.

Emf measurements

The potentiometric titrations were carried out, in 0.15 mol dm^{-3} $NaClO_4$ at 298.1 ± 0.1 K, by using the experimental procedure (burette, potentiometer, cell, stirrer, microcomputer, *etc*.) that has been fully described elsewhere.[9] The acquisition of the emf data was performed with the computer program PASAT.[10] The reference electrode was an Ag/AgCl electrode in saturated KCl solution. The glass electrode was calibrated as an hydrogen-ion concentration probe by titration of well-known amounts of HCl with CO_2-free NaOH solutions and determining the equivalent point by the Gran's method[11] which gives the standard potential, E^o, and the ionic product of water (pK_w = 13.73(1)).

The computer program HYPERQUAD[12] was used to calculate the protonation and stability constants. The DISPO program was used to calculate the distribution plots.[13] The titration curves for each system were treated either as a single set or as separated curves without significant variations in the values of the stability constants. The basicity constants of [21]aneN$_7$ were taken from ref. 14.

The basicity constants of NAD$^+$ and NADP$^+$ were determined under the same experimental conditions.[15] The titration of the systems containing either NAD$^+$ or NADP$^+$ and [21]aneN$_7$ were performed either from acid to basic pH or in the reverse sense in order to check the reversibility of the systems. The pH range used for computing the stability constants was usually 3.0–9.5 and at least three titration curves were performed for each one of the studied systems (*ca.* 250 experimental points, concentrations of [21]aneN$_7$ were 1×10^{-3} mol dm^{-3} and those of the nucleotides were in the range 1×10^{-3} mol dm^{-3} to 3×10^{-3} mol dm^{-3}).

NMR measurements

The ^{1}H and ^{13}C NMR spectra were recorded on Varian UNITY 300 and UNITY 400 spectrometers, operating at 299.95 and 399.95 MHz for ^{1}H and at 75.43 and 100.58 MHz for ^{13}C. The spectra were obtained at room temperature in D_2O solutions. For the ^{13}C NMR spectra dioxane was used as a reference standard (δ = 67.4) and for the ^{1}H spectra the solvent signal was the reference. The ^{31}P NMR spectra were recorded at 121.42 MHz on a Varian UNITY 300 MHz. Chemical shifts are relative to an external reference of 85% H_3PO_4. Adjustments to the desired pH were made using drops of HCl or NaOH solutions. NOE measurements were not possible due to unfavourable correlation times even with the use of spin-lock techniques like ROESY. The pH was calculated from the measured pD values using the correlation, pH = pD − 0.4.[16]

Molecular dynamics calculations

The theoretical calculations have been run in a Power Indigo2 SGI computer, and as forcefield CHARMm MSI version has been used. Two different trajectories for molecular dynamics calculations at 1000 K have been calculated, 100 ps for free NAD$^+$ and NADP$^+$ and $H_4([21]aneN_7)^{4+}$, and 500 ps for the different NAD$^+$–$H_4([21]aneN_7)^{4+}$ and NADP$^+$–$H_4([21]aneN_7)^{4+}$ complexes formed. Adducts with the tetraprotonated macrocycle were selected, since in their pH range of formation, all four protons would be most likely bound to the macrocycle. On the other hand, structural information for this cation was available from the literature,[3] and can be used as a standard check for the conformational calculations.

In energy calculations a 14 Å cut-off distance was employed, with a switching function between 11.0 and 14.0 Å for van der Waals terms. The system was prepared by energy minimisation, 1000 steps of conjugated gradient, 10 ps of heating and equilibration at 1000 K velocity rescaling every 50 fs step. Starting from the final structure of this equilibration a set of dynamic simulations, as previously described, were performed. During the molecular dynamic trajectories a structure was relaxed through energy minimisation at 0 K every 10 ps.

For each molecular dynamics trajectory, free compound lowest energy structures were selected to build up the complex between $H_4([21]aneN_7)^{4+}$ and NAD$^+$ or NADP$^+$. Computing was performed either with dielectric constant $\varepsilon = 1$ or $\varepsilon = 80$ without observing significant differences in the results.

Electrochemistry

Cyclic voltammograms were obtained on a conventional three-electrode cell with a potentiostat (HQ100), a signal generator (Newtronics 200P) and an *x*–*y* recorder (Riken-Denshi F35). A hanging mercury drop electrode (HMDE) (Metrohm AGCH9100), platinum and glassy electrodes were used as working electrodes. A platinum-wire auxiliary electrode and a saturated calomel reference electrode (SCE) completed the standard three-electrode arrangement. The scan rate was varied from 0.01 to 1000 V s^{-1}.

All experiments were carried out under an argon atmosphere in a cell thermostated at 298.0 ± 0.1 K. In all samples $NaClO_4$ 0.15 mol dm^{-3} was used as supporting electrolyte. Before the

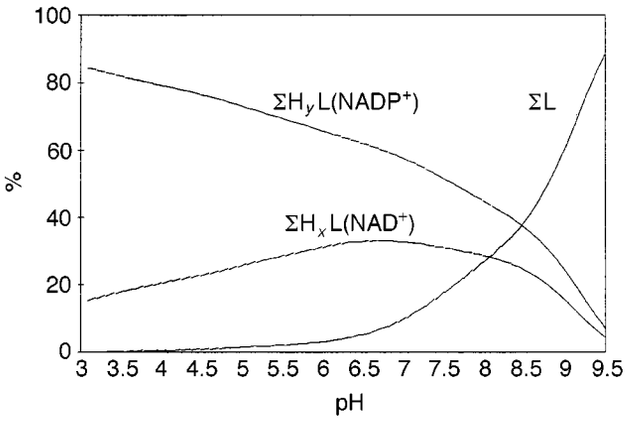

Fig. 1 Calculated distribution diagram for the system $NADP^+$–NAD^+–[21]aneN$_7$ (10^{-3} mol dm^{-3} for all the reagents). Overall amounts of complexed NAD^+, $NADP^+$ and free [21]aneN$_7$ are plotted *versus* pH.

series of runs, solid electrodes were cleaned and activated. Electrochemical pre-treatment was performed in blank solutions by applying +1.50 V *vs.* SCE for 10 min followed by −1 V for 1 min.[17]

Modified carbon paste electrodes were prepared in a conventional manner[18] by thoroughly mixing a 30 mg sample of high purity powdered graphite (Koch Light) and nujol oil in a mortar and pestle. The paste was packed into the tip of a 3 mm diameter holder in contact with the glassy carbon electrode.

Results and discussion

Basicity constants of NAD^+ and $NADP^+$

NAD^+ and $NADP^+$ present, in the pH range 3.0–9.5, one and two protonation steps, respectively (NAD^+, log K_{HA} = 3.88(2); $NADP^+$, log K_{HA} = 5.86, log K_{H_2A} = 3.87(1)). The basicity constant of 3.8 logarithmic units found in both dinucleotides corresponds, as proved by NMR, to protonation of the nitrogen atom labelled as N1 of the adenine moiety. In fact, in the pH range 3–5 ^{13}C signals assigned to carbon atoms A6 and A2 show large variations in chemical shift (for the labelling Scheme 1) while below and above this pH range no further significant variations are observed. First protonation of $NADP^+$ (log K_{HA}= 5.86(1)) occurs, however, on the phosphate group attached to the ribose moiety of the adenine domain. ^{31}P NMR spectra recorded at different pH values show a 5 ppm downfield shift of the singlet signal assigned to this phosphorus in the pH range where this protonation takes place (pH 7–5).

Interaction of NAD^+ and $NADP^+$ with [21]aneN$_7$

Potentiometric studies on the interaction of [21]aneN$_7$ with NAD^+ and $NADP^+$ carried out in the pH range 3.0–9.5, show the formation of adduct species of 1:1 stoichiometry ($H_pLA^{(p-n)}$; L = [21]aneN$_7$, A = NAD^+ or $NADP^+$) with protonation degrees varying from 3 to 7 for NAD^+ and from 3 to 8 for $NADP^+$. The values of the stepwise stability constants ($H_pL^{p+} + A^{n-} = H_pLA^{(p-n)+}$, log K_p) being: NAD^+, log K_3 = 3.15(2), log K_4 = 4.27(3), log K_5 = 5.02(2), log K_6 = 6.62(3) and log K_7 = 7.59(3); $NADP^+$, log K_3 = 3.38(2), log K_4 = 4.74(3), log K_5 = 7.19(2), log K_6 = 10.07(4), log K_7 = 11.84(3) and log K_8 = 9.35(4), K_8 refers to the addition of protonated $NADP^+$ to the heptaprotonated macrocycle. Although the values of the constants obtained for $NADP^+$ are clearly higher than those for NAD^+, the different basicities of both dinucleotides makes it difficult to draw conclusions on the selective recognition of one of them over the other and on the pH range where discrimination is achieved. However, as we have proposed[3,19,20] a distribution diagram for the ternary system NAD^+–$NADP^+$–[21]aneN$_7$ in which the overall amounts of complexed NAD^+ and $NADP^+$ are represented as a function of pH, offers an unambiguous means of establishing selectivity patterns in these kinds of systems. Such a representation (Fig. 1) clearly shows that $NADP^+$ is selectively recognised over NAD^+ by [21]aneN$_7$ throughout the whole pH range studied. The phosphate group attached to the ribose moiety would play an important role since it yields a higher negative charge on $NADP^+$ and can form additional salt bridges with the polyammonium groups of the receptor. ^{31}P NMR proves the participation of this phosphate group in the interaction with protonated [21]aneN$_7$. The resonance of this phosphorus bears an upfield shift of *ca.* 1 ppm when adding an equimolar amount of [21]aneN$_7$ at fixed pH. Higher ratios of $NADP^+$–[21]aneN$_7$ do not yield further shifts which, on the other hand, supports the 1:1 substrate–receptor stoichiometries inferred from the pH-metric titrations.

Table 1 C–C–N–C and C–N–C–C torsion angles for tetraprotonated [21]aneN$_7$

Atoms	RX[a]	Free[b]	Complex[c]
C(3)–C(2)–N(1)–C(21)	160.7	168.1	−86.4
C(2)–N(1)–C(21)–C(20)	−164.4	172.2	−142.4
C(2)–C(3)–N(4)–C(5)	179.9	156.6	139.0
C(3)–N(4)–C(5)–C(6)	179.2	150.6	162.7
C(5)–C(6)–N(7)–C(9)	171.5	−163.1	−164.2
C(6)–N(7)–C(8)–C(9)	175.3	163.1	−101.2
C(8)–C(9)–N(10)–C(11)	−172.5	−150.6	−174.7
C(9)–N(10)–C(11)–C(12)	177.6	156.6	−156.6
C(11)–C(12)–N(13)–C(14)	−167.2	168.1	88.2
C(12)–N(13)–C(14)–C(15)	95.5	102.3	76.3
C(19)–C(15)–N(16)–C(17)	−175.4	169.6	88.4
C(15)–N(16)–C(17)–C(18)	78.6	−46.2	−44.2
C(17)–C(18)–N(19)–C(20)	73.7	−45.8	−173.9
C(18)–N(10)–C(20)–C(21)	61.2	86.9	170.1

[a] Data taken from ref. 3. [b] Average values from 100 ps molecular dynamics calculations for free H$_4$[21]aneN$_7$. [c] Average values from 500 ps molecular dynamics calculations of $NADP^+$(**4**)–H$_4$[21]aneN$_7$.

Molecular dynamics

The calculated structure of the H$_4$([21]aneN$_7$)$^{4+}$ cation agrees quite well with that found in the X-ray structure of the solid compound [21]aneN$_7$·4HCl·H$_2$O.[3] Nevertheless, some slight differences between the X-ray structure and the calculated structure are observed which, most likely, arise from the different crystallisation and molecular simulations conditions.[21]

As from X-ray data, the tetraprotonated macrocycle itself has a boat-shaped ellipsoid form.[3] Torsion angles around the ring (Table 1) can be used to compare calculated and X-ray structures. Although with some deviations with respect to standard values, the average dihedral C–C–N–C angles for the structures of lower energy in molecular dynamics are close to the *trans* configuration around four of the seven nitrogen atoms in the macrocycle (average value 160 ± 20°). Depending on the approach direction, there are two nitrogens with a mixture of *trans* and *gauche* conformations. Finally, the last nitrogen is more appropriately described as being in the *gauche* conformation 60 ± 20°. For example, Fig. 2A shows the lowest energy conformation of H$_4$([21]aneN$_7$)$^{4+}$ from a 100 ps dynamic simulation.

Similarly to the solid state results,[3] intramolecular hydrogen bonding between nitrogens of the macrocycle has not been observed.

In general, nucleosides, nucleotides and their derivatives are very flexible molecules with torsion angles falling in a wide range.[22] For free NAD^+ and $NADP^+$ there were not crystallographic data available in the Cambridge Crystallographic Data Base; the only full set of three-dimensional data found corresponds to NAD^+ co-ordinated to Li^+ and for complexes with proteins of NAD^+ and $NADP^+$. In all these complexes both dinucleotides adopt conformations with energies much higher

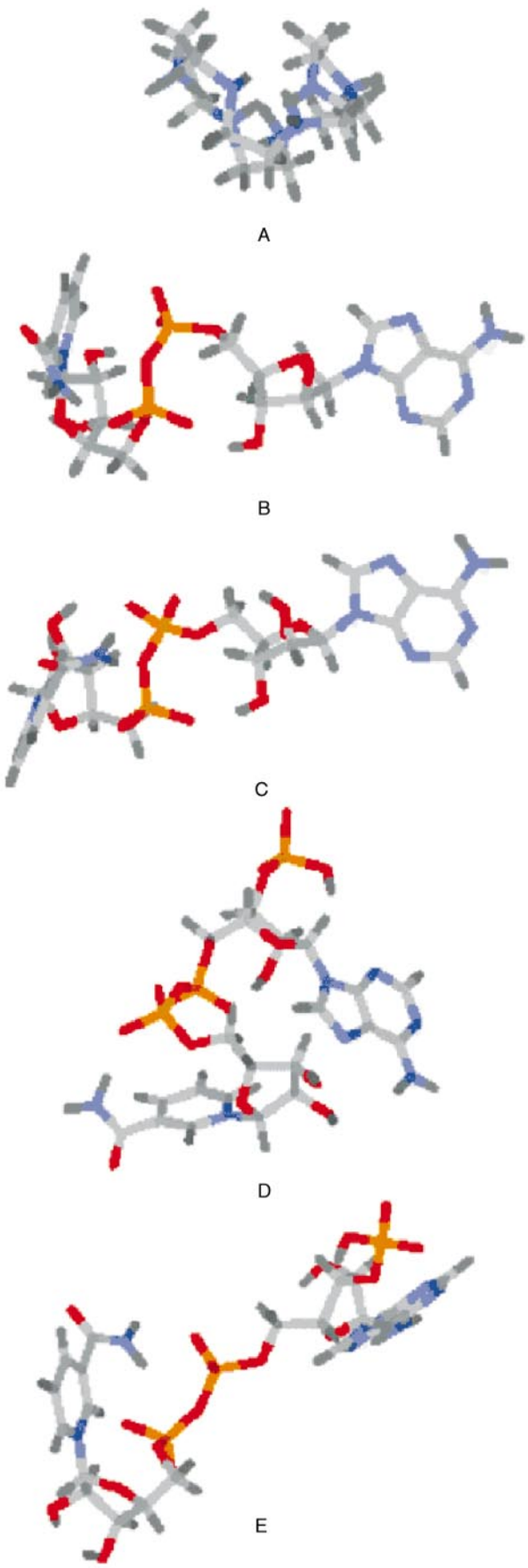

Fig. 2 Lowest energy structures of free compounds from 100 ps dynamic trajectory. (A) $H_4([21]aneN_7)^{4+}$; (B) NAD^+(**1**); (C) NAD^+(**2**); (D) $NADP^+$(**3**) and (E) $NADP^+$(**4**).

than those of the generally accepted "standard low energy structures" of nucleotides.[23] Therefore, owing to the inherent flexibility of NAD^+ and $NADP^+$ a restricted conformational search analysis of torsional angles of the central part of both molecules was carried out. In Table S1, available as supplementary data,† a comparison of NAD^+ and $NADP^+$ in their free forms or as part of protein complexes is presented. Particular attention was focused on the dihedral angles of the adenosine moiety, P1–AO5′–AC5′–AC4′ and AO5′–AC5′–AC4′–AO1′, which can be related to the orientation of the third phosphate group in $NADP^+$ (for the labelling see Scheme 1).

Either for NAD^+ or $NADP^+$ two different structures, representative of a distinct part of conformational space, have been used as free compounds for the initial docking to the macrocycle. Both structures may be considered as the average of two different conformational families. Therefore, four different configurations have been used for the free dinucleotides (NAD^+(**1**), NAD^+(**2**), $NADP^+$(**3**) and $NADP^+$(**4**)). The lowest energy conformations of NAD^+(**1**), NAD^+(**2**), $NADP^+$(**3**) and $NADP^+$(**4**) from 100 ps dynamic trajectory are shown in Figs. 2B–2E.

Although the energy difference between the (**1**) and (**2**) forms for NAD^+ (118.5 kcal mol^{-1}) and the (**3**) and (**4**) forms for $NADP^+$ (83.3 kcal mol^{-1}) is quite significant, conformational analysis using six dihedral angles of the central part of NAD^+ and $NADP^+$ indicates that both configurations are always at the regions of minimum energy, or close to them. However there are quite important energy barriers between some of the dihedral angles of both configurations and these may be critical for conformational interconversion, for instance, between the torsion angles P2–NO5′–NC5′–NC4′ *vs.* P1–AO5′–AC5′–AC4′ for free NAD^+ and $NADP^+$ compounds.

Pentosa rings are important flexible regions in NAD^+ and $NADP^+$ structures, and they should also be considered in the analysis. The furanose conformation of adenosine nucleoside —sugar (**A**)—in NAD^+(**1**) and NAD^+(**2**) is C1′-*exo* (pseudorotation angle, P, average value is 135°). Whereas the other furanose ring—sugar (**N**)—has a typical C1′-*exo* ($P = 139°$) and C2′-*endo* ($P = 166°$) for conformations (**1**) and (**2**) of NAD^+, respectively. $NADP^+$ sugar (**N**) conformations are similar to those in NAD^+, C2′-*endo* ($P = 145°$) and C2′-*endo* ($P = 168°$) for the forms (**3**) and (**4**) of $NADP^+$, respectively. However, $NADP^+$ sugar (**A**) configurations are quite similar to the NAD^+ ones, C4′-*exo* ($P = 48°$) for form (**4**), and C3′-*endo* ($P = 17°$) for form (**3**).

Furanose conformations for both sets of structures (forms (**1**) and (**2**) of NAD^+ and forms (**3**) and (**4**) of $NADP^+$) fall close to or within the two preferred pseudorotation angle regions.[23–25] The P values for sugar (**N**) in NAD^+ and $NADP^+$ are, for forms (**1**), (**2**), (**3**) and (**4**), very close to the standard C2′-*endo* conformation ($144° \leqslant P \leqslant 180°$). However, the inclusion of the phosphate group in the adenosine nucleoside of $NADP^+$ modifies the furanose ring puckering to a C3′-*endo* configuration ($0° \leqslant P \leqslant 36°$) while sugar (**A**) in NAD^+ retains a conformation close to C2′-*endo*.

Once the free compounds had been analysed, the next step was to study the four different complexes. The initial docking of the two distinct NAD^+ and $NADP^+$ forms to $H_4([21]aneN_7)^{4+}$ was empirical; electrostatic and van der Waals forces being the only energetic contributions considered. Molecular dynamics with a trajectory of 500 ps were simulated for each one of the four possible complexes. As previously pointed out, 50 structures (each 10 ps) were minimised. The final comparative conformational analysis was done using the lowest energy complexes.

The 50 minimised structures from 500 ps dynamic trajectories can be clustered in different conformational families, which can be considered as representative of an important collective of configurations. For the four simulated complexes, the cluster of configurations with the lowest co-ordinate rmsd (root mean square deviation) usually includes those conformations with lower energy values. As an example, the 10 structure cluster for the $NADP^+$(**4**)–$H_4([21]aneN_7)^{4+}$ adduct is shown in Fig. 3.

Table 2 Conformational energy values for 500 ps dynamic trajectory for the more stable structures of NAD^+(**1**)–H_4([21]$aneN_7$)$^{4+}$, NAD^+(**2**)–H_4([21]$aneN_7$)$^{4+}$, $NADP^+$(**3**)–H_4([21]$aneN_7$)$^{4+}$ and $NADP^+$(**4**)–H_4([21]$aneN_7$)$^{4+}$ adduct species

	E_A [a]	E_B	E_C	E_D	E_F
NAD^+(**1**)–H_4([21]$aneN_7$)$^{4+}$	−217.9	−383.8	−601.7	−588.6	+13.1
NAD^+(**2**)–H_4([21]$aneN_7$)$^{4+}$	−99.4	−383.8	−493.2	−856.8	−373.6
$NADP^+$(**3**)–H_4([21]$aneN_7$)$^{4+}$	−338.4	−383.8	−722.3	−876.4	−154.1
$NADP^+$(**4**)–H_4([21]$aneN_7$)$^{4+}$	−97.1	−383.8	−490.9	−906.6	−425.7

[a] Energy in kcal mol^{-1}. E_A: conformational energy of forms (**1**), (**2**), (**3**) and (**4**) of free NAD^+ and $NADP^+$. E_B: conformational energy of free H_4([21]$aneN_7$)$^{4+}$. E_C: conformational energy = $E_A + E_B$; E_D = conformational energy of the different complexes. E_F = conformational energy = $E_D - E_C$.

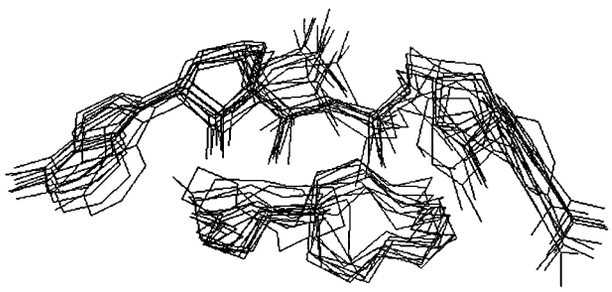

Fig. 3 View of a cluster of 10 structures from 500 ps dynamic simulation, including lowest energy conformation, of $NADP^+$(**4**)–[21]$aneN_7$ complex.

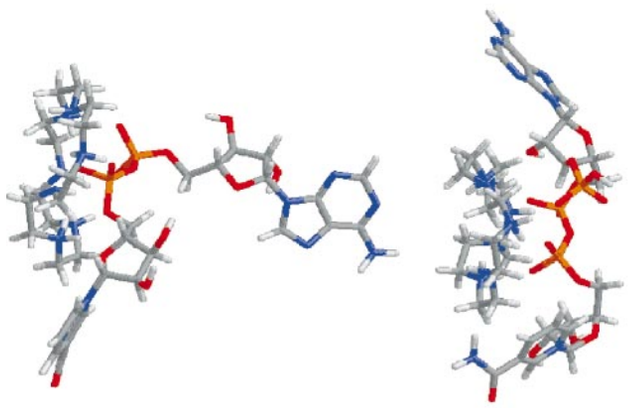

Fig. 4 Structural comparison between NAD^+(**2**)–[21]$aneN_7$ and $NADP^+$(**4**)–[21]$aneN_7$ lowest energy conformations from 500 ps dynamic simulations.

Apart from the lowest energy configuration, the rest of the conformations are among those more stable from an energetic point of view. The rmsd value for the whole set of atoms and 10 configurations is quite low, 0.87.

Thermodynamic stability of NAD^+ and $NADP^+$–macrocycle complexes can be inferred from energy differences between complex and free compounds. The results for the four complexes NAD^+(**1**)–H_4([21]$aneN_7$)$^{4+}$, NAD^+(**2**)–H_4([21]$aneN_7$)$^{4+}$, $NADP^+$(**3**)–H_4([21]$aneN_7$)$^{4+}$, and $NADP^+$(**4**)–H_4([21]$aneN_7$)$^{4+}$ are shown in Table 2.

As can be clearly seen in Table 2, only three of the four complexes studied may be considered as stable ($\Delta E_{complex} < 0$), whereas NAD^+(**1**)–H_4([21]$aneN_7$)$^{4+}$ has $\Delta E_{complex} > 0$. In spite of the significantly lower conformational energies calculated for forms (**1**) and (**3**) in the free dinucleotides, the complexes between forms (**1**) and the macrocycle are less favourable than those with forms (**2**). In other words, complexation with H_4([21]$aneN_7$)$^{4+}$ shifts the dinucleotide conformational equilibrium towards configurations (**2**) and (**4**). The lowest energy complex structures, NAD^+(**2**)–H_4([21]$aneN_7$)$^{4+}$ and $NADP^+$(**4**)–H_4([21]$aneN_7$)$^{4+}$, are shown in Fig. 4. The overall energy difference between both simulated complexes (52 kcal mol^{-1}) agrees with the experimental results pointing out that $NADP^+$ is better recognised by the macrocycle than NAD^+.

In general, the macrocycle displays when complexed a more opened and flattened configuration than when free.[26,27] In this sense, the C–C–N–C torsion angles in the lowest energy complex ($NADP^+$(**4**)–[21]$aneN_7$) are quite different to those found in the free macrocycle (Table 1). Only two of the seven nitrogen atoms are close to the *trans* conformation while the other ones display a mixture between the *trans* and *gauche* configurations depending on the approach direction. The rmsd value range for the comparison between the free and the complexed macrocycle is 2.4–3.5, the higher rmsd value corresponding to the less stable complex (NAD^+(**1**)–H_4([21]$aneN_7$)$^{4+}$).

Likewise, NAD^+ and $NADP^+$ conformations are different in their complexed and free forms. The largest torsion angle modifications correspond to the AO5′–AC5′–AC4′–AO1′ dihedral angles, particularly for $NADP^+$(**4**)–[21]$aneN_7$ complex with the lowest total energy (163.4° in the free form and −32.8° in the complex).

Similarly to NAD^+ and $NADP^+$ free compounds, the search conformational analysis for the six dihedral angles of the central part of both molecules in the complexes shows that both configurations are always at or close to the regions of minimum energy, especially in the case of forms (**2**) and (**4**). Furthermore, for some torsion angles the energy barriers are high enough to avoid a direct interconversion between forms (**1**) and (**2**) and between forms (**3**) and (**4**). These energy barriers are particularly high for dihedral angles P1–AO5′–AC5′–AC4′ *vs.* AO5′–AC5′–AC4′–AO1 either in NAD^+ or $NADP^+$. Both torsion angles are related to the mobility of the adenosine moiety and to the interaction with the macrocycle.

Puckering of furanose rings is significantly modified during complex formation. The smallest changes occur in $NADP^+$ complexes, particularly in $NADP^+$(**4**)–[21]$aneN_7$ (complex with the lowest energy). The configurations of sugar (**A**) in $NADP^+$(**3**)–[21]$aneN_7$ and $NADP^+$(**4**)–[21]$aneN_7$ complexes are C4′-*exo* ($P = 58°$), and O4′-*endo* ($P = 80°$), respectively. In the case of NAD^+(**1**) and NAD^+(**2**)–macrocycle complexes, sugar (**A**) conformations are C1′-*exo* ($P = 121°$), and O4′-*endo* ($P = 85°$), respectively. Sugar (**N**) presents C4′-*exo* ($P = 69°$), C1′-*exo* (O4′-*endo*) ($P = 108°$), C1′-*exo* ($P = 136°$) and C2′-*endo* ($P = 152°$) conformations for NAD^+(**1**), NAD^+(**2**), $NADP^+$ (**3**) and $NADP^+$(**4**)–H_4([21]$aneN_7$)$^{4+}$ complexes, respectively.

In general, pentose configurations in the four complexes are relatively far from the two preferred pseudorotation angles (C3′-*endo* and C2′-*endo*).[21,24] This fact may be partially compensated for by the modification in the hydrogen-bond network,[1c,26,27] and the gain in favourable electrostatic interaction between the phosphate groups and polyammonium groups.

The number of intramolecular hydrogen-bonds (H-bonds) is 3 for free NAD^+(**1**), NAD^+(**2**) and $NADP^+$(**3**), and 6 for $NADP^+$(**4**). The total number of H-bonds (intra- plus intermolecular) increases considerably in the four simulated complexes. All intramolecular H-bonds for the four complexes are located in the NAD^+ and $NADP^+$ dinucleotides. The number of intramolecular hydrogen bonds in NAD^+(**1**)–macrocycle is 3 while there are 10 intermolecular hydrogen bonds between NAD^+ and H_4([21]$aneN_7$)$^{4+}$. For NAD^+(**2**)–macrocycle the number of intra- and intermolecular hydrogen bonds is 0 and

Table 3 Distance between phosphorus atoms of phosphate groups and charged nitrogen atoms in NAD^+(**1**)–H_4([21]$aneN_7$)$^{4+}$, NAD^+(**2**)–H_4([21]$aneN_7$)$^{4+}$, $NADP^+$(**3**)–H_4([21]$aneN_7$)$^{4+}$ and $NADP^+$(**4**)–H_4([21]-$aneN_7$)$^{4+}$ adduct species

		P–N^+ Distance in Å			
		N^+1	N^+7	N^+10	N^+16
NAD^+(**1**)–H_4([21]$aneN_7$)$^{4+}$	P1	3.35	5.46	5.30	4.16
	P2	5.12	3.18	3.15	5.08
NAD^+(**2**)–H_4([21]$aneN_7$)$^{4+}$	P1	5.82	3.51	3.74	6.24
	P2	3.62	3.83	3.70	3.80
$NADP^+$(**3**)–H_4([21]$aneN_7$)$^{4+}$	P1	5.41	3.87	3.60	4.96
	P2	3.76	4.89	5.44	3.21
	P3	9.37	10.96	11.46	10.823
$NADP^+$(**4**)–H_4([21]$aneN_7$)$^{4+}$	P1	4.87	3.21	3.44	3.90
	P2	3.95	5.51	5.74	3.87
	P3	9.72	5.00	3.94	8.03

12, respectively. The number of intramolecular hydrogen bonds is drastically reduced from 3 in free $NADP^+$(**3**) to 0 in the $NADP^+$(**3**)–H_4([21]$aneN_7$)$^{4+}$ complex, which may partially be compensated for by 11 intermolecular hydrogen bonds. Finally for the complex $NADP^+$(**4**)–macrocycle the number of intermolecular hydrogen bonds is 11.

Obviously, another contribution to complex stabilisation is electrostatic interaction between phosphate groups and positively charged nitrogens. The distances between P atoms and charged N for 500 ps dynamics minimum energy structures are shown in Table 3 for the four studied complexes.

In NAD^+(**1**)–H_4([21]$aneN_7$)$^{4+}$ each phosphate group lies close to two adjacent charged nitrogens in a symmetrical orientation (P1 is closer to N4 and N10, and P2 to N16 and N19). In NAD^+(**2**)–H_4([21]$aneN_7$)$^{4+}$, P2 is close and symmetrically positioned with respect to the four charged nitrogens, P1 being close to the contiguous charged nitrogens N16 and N19. The phosphorus atom of the phosphate group hanging from the adenosine moiety (P3) is, in $NADP^+$(**3**)–H_4([21]$aneN_7$)$^{4+}$, far away (>9 Å) from the protonated nitrogens of the macrocycle, whereas the orientation of P1 and P2 is similar to that of P1 and P2 in NAD^+(**1**)–H_4([21]$aneN_7$)$^{4+}$. However, in $NADP^+$(**4**)–macrocycle, P3 is close to the contiguous charged nitrogens N16 and N19, P1 is relatively close to the four charged nitrogens, particularly to N4 and N19, and P2 is pointing towards N10 and N16.

Considering distances P–N $\leqslant$ 5.0 Å as representative of the electrostatic interaction, the larger and the shorter electrostatic contribution correspond to $NADP^+$(**4**)–H_4([21]$aneN_7$)$^{4+}$ and NAD^+(**1**)–H_4([21]$aneN_7$)$^{4+}$ complexes, respectively, which, on the other hand, are the complexes with the lowest and highest total energy. NAD^+(**2**) and $NADP^+$(**3**) complexes with H_4([21]-$aneN_7$)$^{4+}$ have a similar number of P–N distances $\leqslant$ 5.0 Å, although, in general, it seems that those for the second complex are shorter, indicating a possible higher electrostatic favourable contribution. It should be pointed out that in the initial minimised structures used for the molecular dynamic calculations the distance between the adenosine phosphate group in $NADP^+$ and any nitrogen atom of the macrocyclic receptor was always longer than 5 Å.

The global analysis of intermolecular H-bonds formed, and P–N distances (Table 3) can explain the relative stability[1c,26,27] of the four complexes. $NADP^+$(**4**)–H_4([21]$aneN_7$)$^{4+}$ (lowest energy complex) has the largest electrostatic contribution, (interaction of three P with four charged nitrogens) and 11 intermolecular hydrogen bonds. Besides an important electrostatic contribution NAD^+(**2**)–H_4([21]$aneN_7$)$^{4+}$ has the largest number of intermolecular hydrogen bonds. Finally, NAD^+(**1**)–H_4([21]$aneN_7$)$^{4+}$ presents the lowest electrostatic contribution being, hence, the least stable of the four simulated complexes.

A point that deserves particular attention, is the fact that interconversion between the two conformations considered for both dinucleotides is practically prevented in their complexes by the high energy torsional barriers (P1–AO5′–AC5′–AC4′ *vs.* AO5′–AC5′–AC4′–AO1′). In other words, once the adducts are formed, there are important sterically unfavourable interactions which avoid changes from $NADP^+$(**3**) to $NADP^+$(**4**) since this would imply a rotation around torsion angles P1–AO5′–AC5′–AC4′ and AO5′–AC5′–AC4′–AO1′. This may be interpreted as if the equilibrium between conformations (**3**) and (**4**) was partially shifted to configuration (**4**) (lowest energy conformation for free compounds) due to the formation of the more stable $NADP^+$(**4**)–H_4([21]$aneN_7$)$^{4+}$.

Finally, the global analysis of simulation calculations seems to point out that selective recognition of $NADP^+$ over NAD^+ by [21]$aneN_7$ could be largely achieved by the participation of the third additional phosphate group in the adenosine moiety of $NADP^+$. This observation is in good agreement with experimental data and supports the conclusions derived from those results.

Electrochemistry

The electrochemical pattern of NAD^+ and analogue compounds at mercury electrodes in aqueous and non-aqueous media, has been widely studied.[28,29] In neutral alkaline unbuffered solutions of nicotinamide compounds, a first reduction step takes place at −1.08 V *vs.* SCE followed by a second ill-defined cathodic process at −1.3 V. On reversal of the potential scan, an anodic process at −0.17 V is observed.

Unfortunately, mercury electrodes are unable to completely analyse the interaction between nicotinamide compounds and polyammonium macrocycles because addition of stoichiometric amounts of receptor to a nicotinamide solution causes a catalytic effect on the hydrogen discharge that obscures NAD^+ reduction. In addition, new voltammetric peaks appear in the 0.00 to −0.60 V potential range due to the mercury–macrocyclic ligand interaction, which parallels the results reported for analogue macrocyclic compounds.[30]

Accordingly, the electrochemical redox behaviour of NAD^+ and $NADP^+$ has been monitored by cyclic voltammetry at the glassy carbon electrode (GCE). As is depicted in Fig. 5a, in alkaline solutions the main reduction peak (A) appears at −1.28 V and is followed by an ill-defined shoulder (B) near to −1.5 V. An anodic peak (C), poorly defined, was observed at −0.27 V during the subsequent anodic scan. This peak is, however, absent in the initial positive scans, indicating that the oxidation process affects a species generated during prior cathodic steps. In agreement with the literature, peak A corresponds to the one-electron reversible reduction of the oxidised nicotinamide to a radical intermediate, which rapidly dimerises (eqns. (1) and (2)). The dimerisation process inhibits, at least

$$NAD^+ + e^- \rightleftharpoons NAD^\cdot \quad (1)$$

$$2\ NAD^\cdot \rightleftharpoons (NAD)_2 \quad (2)$$

partly, the anodic counterpart (A′) of the electrochemical step (A). At slow sweep rates (v = 0.01–0.50 V s^{-1}), the current function, $i_p/Acv^{1/2}$ remains essentially constant with the scan rate. The peak potential becomes 30 mV per unit of log v more negative while the peak to half-peak potential difference ($E_p - E_p/2$) tends to 40 mV at low scan rates. All these results satisfy the essential diagnostic criteria for a one-electron reversible transfer followed by irreversible dimerisation.[31]

The electrode process B is attributable to the proton-assisted reduction of the $NAD^\cdot$ radical (eqn. (3)), but in part may be

$$NAD^\cdot + H^+ + e^- \rightleftharpoons NADH \quad (3)$$

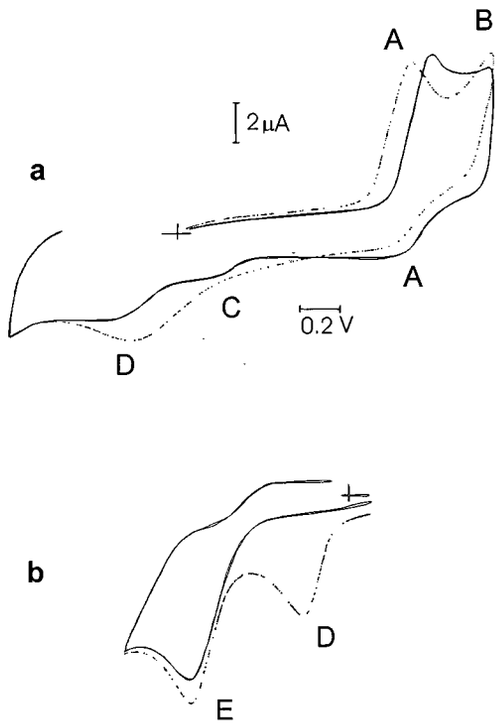

Fig. 5 Cyclic voltammograms at the GCE in neutral solutions a) $NADP^+$ (1.95×10^{-3} mol dm^{-3}) in the absence (continuous line) and in the presence (dotted line) of [21]aneN_7 (3.80×10^{-3} mol dm^{-3}); b) NADH (2.00×10^{-3} mol dm^{-3}); continuous line: initial anodic scan; dotted line: second scan after the potential was extended to −1.5 V *vs.* SCE.

due to the reduction of NAD^+ which diffuses through the depleted layer.[28] Finally, the anodic peak C can be assigned to a one-electron oxidation of the dimeric species to the original nucleotide (eqn. (4)).

$$1/2\ (NAD)_2 \rightleftharpoons NAD^+ + e^- \qquad (4)$$

In neutral and acidic media, the oxidation process C is followed by a second anodic wave (D) at +0.42 V. The intensity of the wave D increases as the switching potential is negatively shifted, suggesting that this electrochemical process involves a product associated to the electrode process B. This is confirmed by the increase in peak current observed after holding the potential at a value close to −1.5 V and then resuming the scan.

It is interesting to note that reduction of NAD^+ and $NADP^+$ at carbon electrodes takes place at potentials 200 mV more negative than at mercury electrodes. Assuming that peak A consists essentially of a one-electron transfer, relatively large values of the diffusion coefficient were obtained (4.2×10^{-6} and 4.0×10^{-6} cm^2 s^{-1} for NAD^+ and $NADP^+$, respectively). In addition, the anodic counterpart of peak A is absent even at fast sweep rates. These features support the hypothesis that a significant portion of the nicotinamide species is reduced to dihydronicotinamide in the −1.2 to −1.5 V potential range at the GCE.

The observed peak potential D agrees with that reported at the pyrolitic graphite electrode in NAD^+ solutions,[28] but it is slightly less positive than the values for the dihydropyridine oxidation in aqueous solution of NADH.[32] Upon repetitive cyclic voltammetry in the extended potential range, the cathodic region remains essentially constant suggesting that NAD^+ is regenerated during anodic steps.

To elucidate the observed electrochemical pattern, the cyclic voltammetric response of NADH and NADPH solutions was studied. It has been well established that these species undergo a two-electron electrochemical oxidation to yield NAD^+ and $NADP^+$ at too positive potentials to allow the use of mercury electrodes. However, the electrochemical processes at solid electrodes are complicated by coupled chemical reactions, adsorption of the reactants onto the electrode surface[32–35] and possible involvement of superficial oxides in hydride abstraction from NADH.[34] This last phenomenon may be responsible for the large background currents observed at carbon and platinum electrodes.[33]

In agreement with the literature, neutral solutions of NADH exhibit a prominent anodic peak (E) at +0.76 V as can be seen in Fig. 5b. This is followed, in the subsequent cathodic scan, by a reduction peak at −1.28 V, corresponding to reduction of the previously generated NAD^+ (process A). In the second and successive scans, an additional peak was observed at +0.33 V. This must be assigned to a typical prepeak,[36] resulting from adsorption of the NAD^+ produced in the oxidation of NADH.[32–35]

The foregoing set of data support the hypothesis that significant amounts of dihydronicotinamide species are generated during the reduction of NAD^+ and $NADP^+$ at carbon electrodes. In addition to surface phenomena, competitive chemical reactions, namely acid catalysed disproportionation of $(NAD)_2$ into NAD^+ and NADH, and hydrolysis of NADH may occur.[37] Accordingly, the electrochemical process D can be tentatively assigned to the NADH oxidation mediated by an adsorbed layer of NAD^+,[38] the overall process possibly being described by eqn. (5).

$$NADH \rightleftharpoons NAD^+ + H^+ + e^- \qquad (5)$$

The presence of adsorbed NAD^+ at the electrode surface may control the overall electrode process in such a way that the electrochemical response is strongly dependent on electrode surface conditioning.[30,31,34,35] In our experimental conditions, it can be expected that adsorption of NAD^+ facilitates $NAD^{\cdot}$ (or NAD^+) reduction to NADH at the expense of the competing radical dimerisation process.

Upon addition of increasing amounts of macrocyclic ligand to a solution of NAD^+ at pH < 9, the reduction wave A is shifted anodically while the oxidation peak C disappears progressively (see Fig. 5a, dotted line). Peak D is in turn displaced toward less positive potentials. For ligand to metal ratios >1 the cyclic voltammetric curves remain almost unchanged, denoting the formation of 1:1 substrate–ligand complex species. The observed shift in the peak potential decidedly increases below pH 10 to a limiting value (typically 50–60 mV) which remains almost pH-independent until pH 3. This result is in accordance with the distribution diagrams calculated from potentiometric data.

As expected, addition of a stoichiometric amount of macrocycle to a solution of NADH leads to an anodic shift of the peak potential (typically 50–60 mV).

Both the morphology and peak current of the cyclic voltammograms for solutions containing the receptor are quite similar to that of NAD^+ or NADH, suggesting that reversible complexation processes occur (eqns. (6) and (7)). Actual data

$$(NAD^+) + LH_q \rightleftharpoons (NAD^+)LH_q \qquad (6)$$

$$(NADH) + LH_q \rightleftharpoons (NADH)LH_q \qquad (7)$$

suggest that adduct formation: a) facilitates the reduction of NAD^+ to NADH whereas subsequent electrode oxidation of dihydropyridine species is hampered by the presence of the macrocyclic ligand, b) it inhibits almost completely the dimerisation reaction (eqn. (2)) at the expense of the dihydronicotinamide formation, and, c) eases the oxidation of NADH presumably mediated by adsorbed NAD^+.

Effect a) can be attributed, at first glance, to an essentially electrostatic effect: upon adduct formation, the species formed became positively charged facilitating electron uptake. Inhibition of dimerisation of the intermediate radical most likely

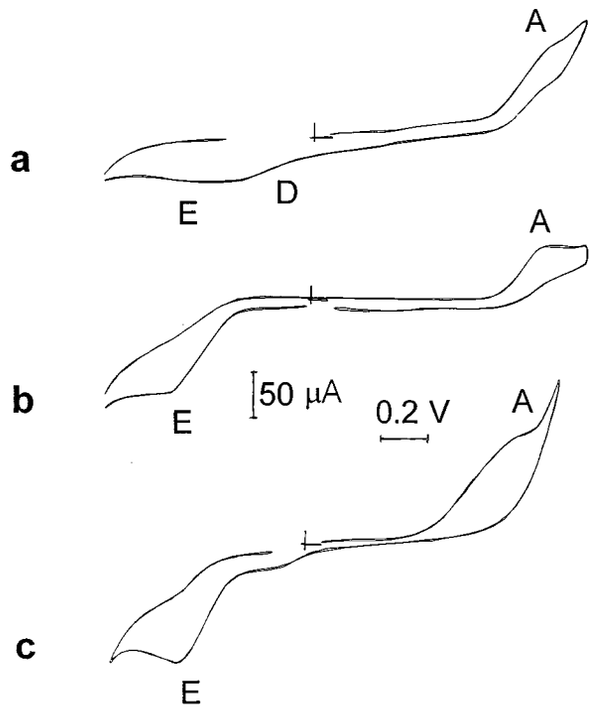

Fig. 6 Cyclic voltammograms at modified carbon-paste electrodes inmersed into a 0.15 mol dm^{-3} $NaClO_4$ solution at pH 7.0. a) NAD^+–MCPE, b) NADH–MCPE, c) NAD^+–[21]aneN$_7$.

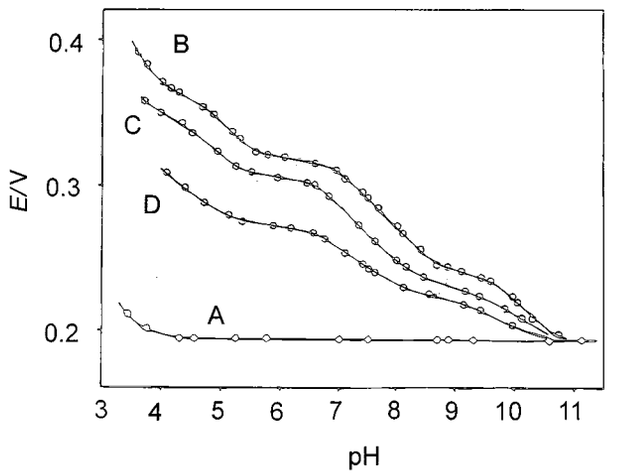

Fig. 7 pH-Dependence of the formal potential of the Fe(III)/Fe(II) couple for solutions containing: (A) $[Fe(CN)_6]^{4-}$ 2.0×10^{-3} mol dm^{-3}; (B) $[Fe(CN)_6]^{4-}$ 2.0×10^{-3} mol dm^{-3} and [21]aneN$_7$ 2.0×10^{-3} mol dm^{-3}; (C) $[Fe(CN)_6]^{4-}$ 2.0×10^{-3} mol dm^{-3}, NAD^+ 2.0×10^{-3} mol dm^{-3} and [21]aneN$_7$ 2×10^{-3} mol dm^{-3}; (D) $[Fe(CN)_6]^{4-}$ 2.0×10^{-3} mol dm^{-3}, $NADP^+$ 2.0×10^{-3} mol dm^{-3} and [21]aneN$_7$ 2×10^{-3} mol dm^{-3}.

results from steric hindrance and an increase in energy barriers associated with the conformational changes required for dimer formation. Finally, effect c) may be explained by assuming that adsorbed NAD^+ acts as a mediator; *i.e.* NADH exchanges the electron with adsorbed NAD^+ which, in turn, exchanges the electron with the electrode. Formation of NAD^+–macrocycle adducts must result in a decrease of the energy barriers associated with such processes, but a detailed study concerning the effect of adduct formation on the electrochemical oxidation of NADH species is in progress.

To minimise adsorption influence, complementary experiments were carried out at modified carbon-paste electrodes (MCPE) immersed into a solution containing supporting electrolyte and eventually macrocyclic receptor. In the last decade, different electrode surface pre-treatments, formation of polymeric films, and modified electrodes have been used as electrochemical sensors.[39] The basic idea is that modified electrodes can preferentially concentrate target analytes from solutions. In MCPE the pre-concentrating agent is incorporated into the surface by mixing it with carbon-paste matrices. Among other procedures,[34,35] poly(thionine)-modified electrodes[40] and conducted polymer electrodes[41] have been used to optimize the analytical oxidation of NADH.

As can be seen in Fig. 6a, after inclusion of powdered NAD^+ into a nujol oil–graphite powder matrix, cyclic voltammograms exhibit an increased signal/background ratio with respect to conventional cyclic voltammograms for NAD^+ solutions at the GCE. Reduction of NAD^+ takes place at similar potentials but the dimer oxidation peak is entirely absent. Fig. 6b presents the cyclic voltammogram for NADH–MCPE. The oxidation process E is clearly observed without adsorption pre-peak D in an initial anodic scan. Subsequent cathodic scans show the reduction peak of NAD^+ supporting the electrochemical pattern previously described. Finally, immersion of NAD^+–MCPE into a solution of the macrocyclic receptor as well as preparation of ligand–NAD^+–MCPE (see Fig. 6c) leads to cyclic voltammograms that present an enhanced NADH oxidation peak after NAD^+ reduction, denoting an almost quantitative NAD^+ to NADH conversion during the electrochemical turnover.

Interaction between NAD^+, $NADP^+$ and [21]aneN$_7$ has been also monitored on the basis of the competitive effect of hexacyanoferrate(II) ions. Competitive methods have been proved of interest for polarographic analysis of metal–ligand equilibria.[42] These methods were applied by Kimura *et al.*[43] for studying the competitive interaction of mercury(II) ions and carboxylate ions with polyammonium receptors. The use of competitive anions for analysing the coordination equilibria between anionic species and receptors was proposed by Lehn *et al.*[44] Earlier electrochemical studies on the complexation of ATP and carboxylate anions with polyammonium receptors on the basis of the competitive effect of the hexacyanoferrate(II) ions have been reported.[19,20]

Cyclic voltammograms of $[Fe(CN)_6]^{4-}$ solutions exhibit a one-electron reversible or quasi-reversible couple without adsorption complications at platinum, carbon and gold electrodes. This electrochemical pattern is altered by adding polyammonium ligands, the morphology of the cyclic voltammograms being heavily dependent on the pH and on the ligand to $[Fe(CN)_6]^{4-}$ molar ratio (L/M). In solutions containing a small excess of receptor, $[Fe(CN)_6]^{4-}$ is fully complexed at pH < 9. As previously described, the complexed species are electroactive and are oxidised almost reversibly at more positive potentials than hexacyanoferrate(II) ions.[19,20,44–46]

For our purposes, the relevant point to emphasise is that addition of a competitive anion, such as NAD^+ or $NADP^+$, produces a shift of the electrochemical parameters from those of the limiting cyclic voltammogram for the hexacyanoferrate(II)–ligand complex to those of uncomplexed $[Fe(CN)_6]^{4-}$. This can be seen for example in Figs. 7 and 8, which represent the pH dependence of the apparent formal potentials and mean diffusion coefficients determined from the cyclic voltammograms for solutions of uncomplexed hexacyanoferrate(II) (curves A), $[Fe(CN)_6]^{4-}$ and ligand (curves B), and $[Fe(CN)_6]^{4-}$, ligand and NAD^+ (and $NADP^+$) in identical total concentrations (curves C and D).

Then, analysis of the electrochemical parameters of the $[Fe(CN)_6]^{3-}/[Fe(CN)_6]^{4-}$couple, namely peak potentials and currents, allows an estimate of the complexation of $[Fe(CN)_6]^{4-}$ by polyammonium receptor since both $[Fe(CN)_6]^{4-}$ and $[Fe(CN)_6]^{4-}$–H_qL adducts display reversible one-electron electrochemical processes. The cyclic voltammetric pattern corresponds to the general case of a system with different electroactive species, which differ in their formal potentials and diffusion coefficients.[47] For this type of system a series of procedures for determining equilibrium constants from the

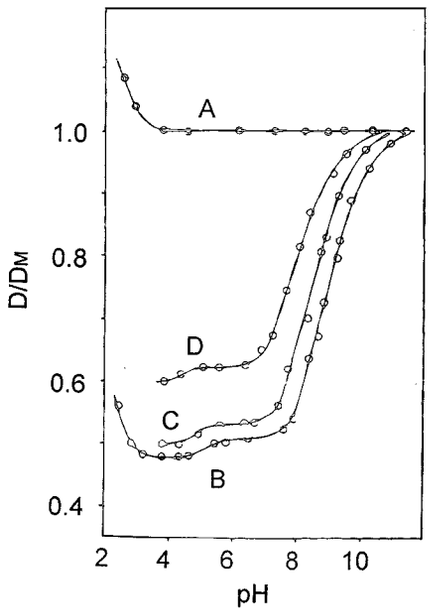

Fig. 8 Variation with the pH of the mean diffusion coefficient calculated from the cyclic voltammograms for solutions containing: (A) $[Fe(CN)_6]^{4-}$ 2.0×10^{-3} mol dm^{-3}; (B) $[Fe(CN)_6]^{4-}$ 2.0×10^{-3} mol dm^{-3} and [21]aneN$_7$ 2.0×10^{-3} mol dm^{-3}; (C) $[Fe(CN)_6]^{4-}$ 2.0×10^{-3} mol dm^{-3}, NAD^+ 2.0×10^{-3} mol dm^{-3} and [21]aneN$_7$ 2×10^{-3} mol dm^{-3}; (D) $[Fe(CN)_6]^{4-}$ 2.0×10^{-3} mol dm^{-3}, $NADP^+$ 2.0×10^{-3} mol dm^{-3} and [21]aneN$_7$ 2×10^{-3} mol dm^{-3}.

measurement of mean diffusion coefficients are available.[48] The Cottrell-type analysis of the diffusive portion of the cyclic voltammograms,[49] as well as direct chronoamperometric measurements enable us to determine the mean diffusion coefficient for a mixture of electroactive species in equilibrium. In solutions containing NAD^+, $[Fe(CN)_6]^{4-}$, and the receptor, calculations based on the generalisation of the molar-ratio are applicable for determining the NAD^+–L stoichiometry.[50–52] The values of selected stepwise stability constants were calculated and agreed with those determined potentiometrically; NAD^+, log $K_4 = 4.3(2)$, log $K_5 = 4.9(2)$; $NADP^+$, log $K_4 = 4.6(2)$, log $K_5 = 7.0(2)$. In addition, the Viossat method provides a direct estimate of the stoichiometry and number of protons (w) involved in the first pH-dependent complexation step.[53,54] Values of log K and w in close agreement with potentiometric data were found (NAD^+; log $K_3 = 2.9(1)$; $NADP^+$; log $K_3 = 3.2(1)$.

Conclusions

[21]aneN$_7$ in its protonated forms interacts in aqueous solution with NAD^+ and $NADP^+$ forming adduct species of 1 : 1 stoichiometry which predominate in solution below pH 9. The stability constants for the interaction of [21]aneN$_7$ with $NADP^+$ are clearly higher, and mixed distribution diagrams show that it is selectively recognised over NAD^+ by the polyammonium receptor throughout a wide pH range. ^{31}P NMR spectra of solutions of the adducts suggest that one of the clues in the selective recognition of $NADP^+$ is the involvement of the phosphate group esterified to the 2′-hydroxy group of the AMP moiety of $NADP^+$ in the interaction with the receptor. Molecular dynamics studies carried out on the interaction of tetraprotonated [21]aneN$_7$ with NAD^+ and $NADP^+$ confirm the participation of the extra phosphate group of $NADP^+$ in the recognition process. In fact, the most stable family of conformers for the $NADP^+$–H_4([21]aneN$_7$)$^{4+}$ shows that this phosphate group interacts strongly with the two adjacent ammonium groups present in the tetraprotonated receptor which would be the factor responsible for the selective recognition of $NADP^+$ over NAD^+. Interaction of NAD^+, $NADP^+$ with the macrocyclic receptor decreases their observed reduction potentials whereas the observed oxidation potentials of NADH and NADPH are shifted toward more positive values. Formation of receptor–nicotinamide dinucleotide adducts alters the electrochemical mechanism for NAD^+ and $NADP^+$ reduction at carbon electrodes, favouring the formation of dihydronicotinamide species rather than that of the dimer species.

Acknowledgements

We are indebted to the DGICYT (PB96-0792-CO2-01) and Generalitat Valenciana Project No. GV-D-CN-09-140 for financial support.

References

1 Some examples of this chemistry are: (*a*) F. P. Schmidtchen, *Top. Curr. Chem.*, 1986, **132**, 101; (*b*) J.-M. Lehn, *Angew. Chem.*, *Int. Ed. Engl.*, 1988, **27**, 89; (*c*) M. P. Mertes and K.-B. Mertes, *Acc. Chem. Res.*, 1990, **23**, 413; (*d*) A. V. Eliseev and H.-J. Schneider, *J. Am. Chem. Soc.*, 1994, **116**, 6081; (*e*) B. Dietrich, *Pure Appl. Chem.*, 1993, **65**, 1457.
2 M. W. Hosseini, J.-M. Lehn and M. P. Mertes, *Helv. Chim. Acta*, 1983, **66**, 2454.
3 A. Bencini, A. Bianchi, E. C. Scott, M. Morales, B. Wang, E. García-España, T. Deffo, F. Takusagawa, M. P. Mertes, K.-B. Mertes and P. Paoletti, *Bioorg. Chem.*, 1992, **20**, 8.
4 A recent study on the interaction of NAD^+ and polyphosphate anions with a receptor containing guanidinium groups is: P. Schiessl and F. P. Schmidtchen, *J. Org. Chem.*, 1994, **59**, 509.
5 H. Fenniri, M. W. Hosseini and J.-M. Lehn, *Helv. Chim. Acta*, 1997, **80**, 786.
6 Articles describing NAD^+ and $NADP^+$ binding sites in enzymes are for example: (*a*) M. J. Adams, M. Buehner, K. Chandrasekar, G. C. Ford, M. L. Hakert, A. Liljas, M. G. Rossman, I. E. Smily, W. S. Allison, J. Everse, N. O. Kaplan and S. S. Taylor, *Proc. Natl. Acad. Sci. USA*, 1973, **70**, 1968; (*b*) N. S. Scrutton, A. Berry and R. N. Perham, *Nature*, 1990, **340**, 39; (*c*) I. Gibbons, B. H. Gibbons, G. Mocz and D. J. Asai, *Nature*, 1991, **352**, 640; (*d*) J. Kuriyan, T. S. R. Krishna, L. Wong, B. Guenther, A. Pahler and C. H. Williams, Jr., *Nature*, 1991, **352**, 172; (*e*) J.-M. Rondeau, F. Tete-Favier, A. Podjarny, J.-M. Reyman, P. Barth, J.-F. Biellman and D. Moras, *Nature*, 1992, **35**, 469.
7 A. Bianchi, M. Micheloni and P. Paoletti, *Inorg. Chem.*, 1985, **24**, 3702.
8 M. Micheloni, P. May and D. R. Williams, *J. Inorg. Nucl. Chem.*, 1978, **40** 1209.
9 E. García-España, M.-J. Ballester, F. Lloret, J.-M. Moratal, J. Faus and A. Bianchi, *J. Chem. Soc.*, *Dalton Trans.*, 1988, 101.
10 M. Fontanelli and M. Micheloni, *Proceedings of the I Spanish-Italian Congress on Thermodynamics of Metal Complexes*, Peñíscola, Spain, 1990, published by Diputación de Castellón. Program for the automatic addition of thew burette additions and electromotive force readings.
11 G. Gran, *Analyst* (*London*), 1952, **77**, 661; F. J. Rossotti and H. J. Rossotti, *J. Chem. Educ.*, 1965, **42** , 375.
12 A. Sabatini, A. Vacca and P. Gans, *Coord. Chem. Rev.*, 1992, **120**, 389.
13 A. Vacca. University of Florence. Unpublished work, FORTRAN program to determine from the stability constants and mass balance equation the distribution of species in multiequilibria systems.
14 A. Bencini, A. Bianchi, P. Dapporto, E. García-España, M. Micheloni and P. Paoletti, *Inorg. Chem.*, 1989, **28**, 1188.
15 A previous study on the basicity constants of NAD^+ and $NADP^+$ can be found in: T. N. Briggs and J. E. Stuehr, *Anal. Chem.*, 1975, **47**,12, 1916.
16 A. K. Covington, M. Paabo, R. M. Robinson and R. G. Bates, *Anal. Chem.*, 1968, **40**, 700.
17 R. C. Engstrom, *Anal. Chem.*, 1982, **54**, 2310.
18 R. N. De Guzmán, Y.-F. Shen, B. R. Shaw, S. L. Suib and C. L. O'Young, *Chem. Mater.*, 1993, **5**, 1395.
19 A. Bencini, A. Bianchi, M. I. Burguete, P. Dapporto, A. Doménech, E. García-España, S. V. Luís, P. Paoli and J. A. Ramírez, *J. Chem. Soc.*, *Perkin Trans. 2*, 1994, 569.
20 A. Andrés, J. Aragó, A. Bencini, A. Bianchi, A. Doménech, V. Fusi, E. García-España, P. Paoletti and J. A. Ramírez, *Inorg. Chem.*, 1993, **32**, 3418.
21 W. F. van Gusteren and H. J. C. Berendsen, *Angew. Chem.*, *Int. Ed. Engl.*, 1990, **29**, 992.

22 S. R. Holbrook, J. L. Sussman, R. W. Warrant and S.-H. Kim, *J. Mol. Biol.*, 1978, **123**, 631.
23 B. S. Reddy, W. Saenger, K. Mühlegger and G. Weimann, *J. Am. Chem. Soc.*, 1981, **103**, 907.
24 C. Altona and M. Sundaralingam, *J. Am. Chem. Soc.*, 1972, **94**, 8205.
25 K. Wüthrich, *NMR of Proteins and Nucleic Acids*, John Wiley and Sons, New York, 1986.
26 G. Papoyan, K.-J. Gu, J. Wiorkiewicz-Kuczera, K. Kuczera and K. Bowman-James, *J. Am. Chem. Soc.*, 1996, **118**, 1354.
27 L. Quian, Z. Sun, J. Gao, B. Movassagh, L. Morales and K.-B. Mertes, *J. Coord. Chem.*, 1991, **23**, 155.
28 (*a*) A. L. Underwood and J. N. Burnett, *Electroanalytical Chemistry*, vol. 6, A. J. Bard ed., Marcel Dekker, New York, 1972, pp. 1–85; (*b*) J. N. Burnett and A. L. Underwood, *Biochem.*, 1965, **4**, 2060; (*c*) J. N. Burnett and A. L. Underwood, *J. Org. Chem.*, 1965, **30**, 1154; (*d*) B. Janik and P. J. Elving, *Chem. Rev.*, 1968, **68**, 295; (*e*) C. O. Schmakel, K. S. V. Santhanam and P. J. Elving, *J. Am. Chem. Soc.*, 1975, **75**, 5083.
29 K. S. V. Santhanam and P. J. Elving, *J. Am. Chem. Soc.*, 1975, **75**, 5482.
30 (*a*) M. Kodama and E. Kimura, *J. Chem. Soc.*, *Dalton Trans.*, 1976, 2335; (*b*) M. Kodama and E. Kimura, *J. Chem. Soc.*, *Dalton Trans.*, 1978, 1081; (*c*) E. Kimura, A. Sakonaka, T. Yatsunami and M. Kodama, *J. Am. Chem. Soc.*, 1981, **103**, 3041.
31 (*a*) J. M. Saveant and E. C. R. Vianello, *Acad. Sci. Paris*, 1963, **256**, 2597; (*b*) R. S. Nicholson, *Anal. Chem.*, 1965, **37**, 667.
32 (*a*) J. Moiroux and P. J. Elving, *J. Am. Chem. Soc.*, 1980, **102**, 6533; (*b*) W. J. Blaedel and R. A. Jenkins, *Anal. Chem.*, 1975, **47**, 1337.
33 (*a*) R. D. Braun, K. S. V. Santhanam and P. J. Elving, *J. Am. Chem. Soc.*, 1975, **97**, 5083; (*b*) J. Moiroux and P. J. Elving, *Anal. Chem.*, 1979, **51**, 346; (*c*) J. Moiroux and P. J. Elving, *J. Electroanal. Chem.*, 1979, **102**, 93.
34 (*a*) P. Hapiot, J. Moiroux and J. M. Savéant, *J. Am. Chem. Soc.*, 1990, **112**, 1337; (*b*) D. Lasr and M. Ariel, *J. Electroanal. Chem.*, 1974, **52**, 291.
35 S. Fukusumi, S. Koumitsu, K. Hironaka and T. Tanaka, *J. Am. Chem. Soc.*, 1987, **109**, 305.
36 A. J. Bard and L. R. Faulkner, *Electrochemical Methods*, Wiley, New York, 1990; R. H. Wopschall and Y. Shain, *Anal. Chem.*, 1967, **39**, 1514.
37 In general, there has been a failure to oxidize NADH cleanly at solid electrodes. However, it is well established that the first step in the electrochemical oxidation of NADH consists of an irreversible electron transfer. The resulting cation radical $NADH^{\bullet +}$ loses a proton to form the neutral radical $NAD^{\cdot}$ which may participate in a second electron transfer (ECE mechanism) or in a homogeneous reaction with $NADH^{\bullet +}$ yielding NAD^{+}. This disproportionation or half-regeneration mechanism (DISP1) has been well characterized for model compounds in organic solvents. See refs. 34, 35.
38 A. P. F. Turner, L. Karube and G. S. Wilson, eds. *Biosensors, Fundamentals and Applications*, Oxford University Press, 1987.
39 W. T. Bresnaham and P. J. Elving, *Biochem. Biophys. Acta*, 1981, **678**, 151.
40 T. Osaka, K. Tanaka and K. Tokuda, *J. Chem. Soc.*, *Chem. Commun.*, 1993, 222.
41 M. Somasandrum and J. V. Bannister, *J. Chem. Soc.*, *Chem. Commun.*, 1993, 1629.
42 G. Schwarzenbach, R. Gut and G. Anderegg, *Helv. Chim. Acta*, 1954, **37**, 937.
43 E. Kimura, A. Sakonaka, T. Yatsunami and M. Kodama, *J. Am. Chem. Soc.*, 1981, **103**, 3041.
44 F. Peter, M. Gross, M. W. Hosseini, J.-M. Lehn and R. B. Sessions, *J. Chem. Soc.*, *Chem. Commun.*, 1981, 1967.
45 (*a*) A. Bencini, A. Bianchi, M. I. Burguete, A. Doménech, E. García-España, S. V. Luís, M. A. Niño and J. A. Ramírez, *J. Chem. Soc.*, *Perkin Trans. 2*, 1991, 1445; (*b*) J. Aragó, A. Bencini, A. Bianchi, A. Doménech and E. García-España, *J. Chem. Soc.*, *Dalton Trans.*, 1991, 319.
46 F. Peter, M. Gross, M. W. Hosseini and J.-M. Lehn, *J. Electroanal. Chem.*, 1983, **144**, 279.
47 (*a*) K. B. Oldham, *J. Electroanal. Chem.*, 1991, **313**, 3; (*b*) D. N. Blauch and F. C. Anson, *J. Electroanal. Chem.*, 1991, **309**, 313.
48 (*a*) V. Kacena and L. Matousek, *Collect. Czech. Chem. Commun.*, 1953, **18**, 294; (*b*) D. R. Crow, *J. Electroanal. Chem.*, 1968, **16**, 137; (*c*) D. R. Crow, *Talanta*, 1982, **29**, 733; (*d*) D. R. Crow, *Talanta*, 1982, **29**, 739; (*e*) D. R. Crow, *Talanta*, 1983, **30**, 659; (*f*) D. R. Crow, *Talanta*, 1986, **33**, 553.
49 (*a*) R. S. Nicholson, *Anal. Chem.*, 1965, **37**, 667; (*b*) D. S. Polcyn and I. Shain, *Anal. Chem.*, 1966, **38**, 370; (*c*) G. Cinzburg, *Anal. Chem.*, 1978, **50**, 375; (*d*) G. Bontempelli, F. Magno and S. Daniele, *Anal. Chem.*, 1985, **57**, 1503.
50 A. Beltrán, D. Beltrán, A. Cervilla and J. A. Ramírez, *Talanta*, 1983, **30**, 124.
51 J. H. Yoe and A. L. Jones, *Ind. Eng. Chem. Anal. Ed.*, 1944, **16**, 11.
52 A. Bianchi, A. Doménech, E. García-España and S. V. Luís, *Anal. Chem.*, 1993, **65**, 3137.
53 B. Viossat, *Rev. Chim. Miner.*, 1972, **9**, 737.
54 A. Doménech, E. García-España and J. A. Ramírez, *Talanta*, 1995, **42**, 163.

Paper 8/06004E